Hot-electron effect in spin dephasing in *n*-type GaAs quantum wells

M. Q. Weng,[1,2] M. W. Wu,[1,2,*] and L. Jiang[2]
[1]*Hefei National Laboratory for Physical Sciences at Microscale, University of Science and Technology of China, Hefei, Anhui 230026, China*
[2]*Department of Physics, University of Science and Technology of China, Hefei, Anhui 230026, China*
(Received 8 January 2004; published 24 June 2004)

We perform a study of the effect of the high in-plane electric field on spin precession and spin dephasing due to the D'yakonov–Perel' mechanism in *n*-type GaAs (100) quantum wells by constructing and numerically solving kinetic Bloch equations. We self-consistently include all scattering such as electron/phonon, electron /nonmagnetic impurity as well as electron–electron Coulomb scattering in our theory and systematically investigate how the spin precession and spin dephasing are affected by the high electric field under various conditions. The hot-electron distribution functions and spin correlations are calculated rigorously in our theory. It is found that the D'yakonov–Perel' term in the electric field provides a nonvanishing effective magnetic field that alters the period of spin precession. Moreover, spin dephasing is markedly affected by the electric field. The important contribution of the electron–electron scattering to spin dephasing is also discussed.

DOI: 10.1103/PhysRevB.69.245320 PACS number(s): 72.25.Rb, 72.20.Ht, 71.10.−w, 67.57.Lm

I. INTRODUCTION

Spintronics is an active field in which processes that manipulate the spin degree of freedom of electrons, with the goal of developing new electronic devices with improved performance and new functionality compared to traditional ones which are based on precise control of the charge distribution of electrons, are studied.[1,2] Understanding spin dephasing is an important prerequisite for the realization of such devices. As most of the semiconductor electronic devices are very small and even a small applied voltage gives a strong electric field, these devices usually work in the hot-electron condition.[3,4] Therefore understanding spin dephasing in the presence of a strong electric field is of particular importance to spintronic application.

Recent experiments have shown that the electron spin lifetime is very long in *n*-type zinc-blende semiconductors.[5–7] In theory spin dephasing in semiconductors without a high electric field has been extensively studied. Three spin dephasing mechanisms have been proposed:[8] the Elliot–Yaffet mechanism[9,10] which is important in the narrow-band-gap and/or high impurity-doped semiconductors; the Bir–Aronov–Pikus mechanism[11] which is important in pure or *p*-type semiconductors; and the D'yakonov–Perel' (DP) mechanism[12] which is the main spin-dephasing mechanism in *n*-type zinc-blende semiconductors such as GaAs and InAs. The DP mechanism originates from spin–orbit interaction in crystal without an inversion center and results in spin splitting of the conduction band at $k \neq 0$. This is equivalent to an effective magnetic field acting on the spin, with its magnitude and orientation depending on the electron wave vector. Moreover, an important many-body spin dephasing mechanism due to combined effects of the inhomogeneous broadening of the spin precession and the spin conserving scattering by irreversibly disrupting the phases between spin dipoles has been proposed recently[13] and closely studied.[14–17]

The study of the effect of electric fields on electron spin in semiconductors is just beginning. Experiments have shown that spin polarization is not destroyed by the strong electric field applied in transport up to a few kV/cm.[18,19] It is revealed that under the right configurations the electric field can drive the electrons toward a larger spin injection length.[2,20–26] In Ref. 27, the spin dephasing in quantum wires under high electric field was studied through Monte-Carlo simulation. Electric manipulation of the spin of two-dimensional (2D) electrons through Rashba[28] spin–orbital interactions using the in-plane ac electric field has also been proposed.[29] Nonetheless how the hot-electron effect affects spin dephasing/transport is so far not fully investigated. Complete understanding of the hot-electron effect on spin dephasing in *n*-type GaAs quantum wells (QWs) can be obtained by solving the many-body kinetic Bloch equations[13,14,30] which have been applied successfully to the study of spin dephasing[17] and spin transport recently.[31,32]

In this paper, we use many-body kinetic equations to study the effect of high electric field on spin dephasing. The paper is organized as follows: In Sec. II we present the model and construct the kinetic Bloch equations. Then we show the effect of the electric field on the spin dephasing problem by numerically solving the kinetic equations. In Sec. III A we first discuss how the electric field affects spin precession. Then we concentrate on understanding the effect of high electric field on spin dephasing under various conditions, such as at different impurity densities, temperatures, and initial spin polarizations. We summarize the main results in Sec. IV. In Appendix A we present the effect of the electron–electron Coulomb scattering on the spin dephasing.

II. MODEL AND KINETIC EQUATIONS

We start our investigation with an *n*-type (100) GaAs QW of width a with its growth direction along the z axis. A uniform electric field **E** and a moderate magnetic field **B** are applied along the x axis (Voigt configuration). Due to confinement of QW, the momentum along the z axis of electrons

is quantized. Therefore the electrons are characterized by a subband index n and a two-dimensional momentum $\mathbf{k}=(k_x,k_y)$, together with spin index $\sigma(=\pm 1/2)$. For simplicity, we only consider wells of small width so that the separation of the subband energy is large enough and therefore only the lowest subband is populated and the transition to the upper subbands is unimportant. It is noted that due to the so called "runaway" effect, the single subband model is valid only when the electric field is less than a few kV/cm.[33,34] This is because when the electric field is above the threshold value, electrons gain energy from the field faster than they can dissipate it by emitting phonons and therefore the transition to upper subbands becomes significant. Consequently in the present paper we only study the case with electric field up to 1 kV/cm which is sufficiently large to produce the hot-electron effect.

For n-type samples, spin dephasing mainly comes from the DP mechanism.[8,12] With the DP term included, the Hamiltonian of the electrons in the QW is given by

$$H=\sum_{\mathbf{k}\sigma\sigma'}\left\{(\varepsilon_{\mathbf{k}}-e\mathbf{E}\cdot\mathbf{R})\delta_{\sigma\sigma'}+[g\mu_B\mathbf{B}+\mathbf{h}(\mathbf{k})]\cdot\frac{\boldsymbol{\sigma}_{\sigma\sigma'}}{2}\right\}c^{\dagger}_{\mathbf{k}\sigma}c_{\mathbf{k}\sigma'}+H_I. \tag{1}$$

Here $\varepsilon_{\mathbf{k}}=\mathbf{k}^2/2m^*$ is the energy spectrum of the electron with momentum $\mathbf{k}$ and effective mass m^*. $\boldsymbol{\sigma}$ is the Pauli matrix. $\mathbf{R}=(x,y)$ is the position. $\mathbf{h}(\mathbf{k})$ represents the DP term which serves as an effective magnetic field with its magnitude and direction depending on $\mathbf{k}$. It is composed of the Dresselhaus term[35] and the Rashba term.[28] For GaAs QWs, the leading term is the Dresselhaus term which can be written as

$$h_x(\mathbf{k})=\gamma k_x(k_y^2-\langle k_z^2\rangle);$$

$$h_y(\mathbf{k})=\gamma k_y(\langle k_z^2\rangle-k_x^2);$$

$$h_z(\mathbf{k})=0. \tag{2}$$

Here $\langle k_z^2\rangle$ represents the average of the operator $-(\partial/\partial z)^2$ over the electronic state of the lowest subband and is therefore $(\pi/a)^2$. $\gamma=(4/3)(m^*/m_{cv})(1/\sqrt{2m^{*3}E_g})(\eta/\sqrt{1-\eta/3})$ and $\eta=\Delta/(E_g+\Delta)$, in which E_g denotes the band gap; Δ represents spin–orbit splitting of the valence band; and m_{cv} is a constant close in magnitude to free electron mass m_0.[36] The Rashba term is proportional to the total electric field. For narrow band-gap semiconductors such as InAs, the Rashba term dominates. For wide band-gap semiconductors like GaAs, it is marginal in the regime of the applied electric field we studied. The interaction Hamiltonian H_I is composed of Coulomb interaction H_{ee}, electron–phonon scattering H_{ph}, as well as electron–impurity scattering H_i. Expressions for them can be found in textbooks.[37,38]

In order to study the hot-electron effect on spin dephasing, we limit our system to a spacial homogeneous one in order to avoid additional complications such as charge/spin diffusion. The kinetic Bloch equations in such a system are constructed using the nonequilibrium Green function method with gradient expansion[38] and can be written as

$$\dot{\rho}_{\mathbf{k},\sigma\sigma'}-e\mathbf{E}\cdot\boldsymbol{\nabla}_{\mathbf{k}}\rho_{\mathbf{k},\sigma\sigma'}=\dot{\rho}_{\mathbf{k},\sigma\sigma'}|_{\mathrm{coh}}+\dot{\rho}_{\mathbf{k},\sigma\sigma'}|_{\mathrm{scat}}, \tag{3}$$

where $\rho_{\mathbf{k}\sigma\sigma'}$ represents the single particle density matrix elements. The diagonal terms describe the electron distribution functions $\rho_{\mathbf{k},\sigma\sigma}\equiv f_{\mathbf{k}\sigma}$. The off-diagonal elements $\rho_{\mathbf{k},1/2-1/2}=\rho^*_{\mathbf{k},-1/21/2}\equiv\rho_{\mathbf{k}}$ stand for the interspin-band polarizations (spin coherence).[30] The second terms in the kinetic equations describe the momentum and energy input from electric field $\mathbf{E}$. $\dot{\rho}_{\mathbf{k}\sigma\sigma'}|_{\mathrm{coh}}$ on the right-hand side of the equations describes the coherent spin precession around applied magnetic field $\mathbf{B}$, the effective magnetic field $\mathbf{h}(\mathbf{k})$ from the DP term as well as the effective magnetic field from electron–electron interaction in the Hartree–Fock approximation. $\dot{\rho}_{\mathbf{k}\sigma\sigma'}|_{\mathrm{scat}}$ denotes the electron–impurity, the electron–phonon, as well as the electron–electron scattering. The expressions for these terms are given in Appendix B.

The initial conditions at $t=0$ are taken to be $\rho_{\mathbf{k}}(0)=0$ and electron distribution functions are chosen to be those of the steady state under the electric field but without the magnetic field and the DP term. Specifically $f_{\mathbf{k},\sigma}(0)$ is the steady solution of kinetic equations (3) with spin coherence $\rho_{\mathbf{k}}$, the magnetic field and the DP term set to zero. These initial distribution functions can be approached by assuming that at time $-t_0$ there is no spin coherence $\rho_{\mathbf{k}}(-t_0)=0$ and the electron distributions are just the Fermi distribution functions for each spin σ at background temperature T:

$$f_{\mathbf{k}\sigma}(-t_0)=\{\exp[(\varepsilon_{\mathbf{k}}-\mu_\sigma)/T]+1\}^{-1}, \tag{4}$$

and then self-consistently solving kinetic equations (3) with the magnetic field and the DP term turned off (therefore no spin precession and $\rho_{\mathbf{k}}\equiv 0$). By taking t_0 large enough one may get the steady state solution before $t=0$. In Appendix A we present a typical electron distribution function in the steady state under the electric field. The imbalance of the the chemical potential $\mu_{1/2}\neq\mu_{-1/2}$ gives the initial spin polarization,

$$P=\frac{N_{e1/2}(0)-N_{e-1/2}(0)}{N_{e1/2}(0)+N_{e-1/2}(0)}, \tag{5}$$

where $N_{e\sigma}(t)=\Sigma_{\mathbf{k}}f_{k,\sigma}(t)$ is the number of the electrons with spin σ at time t.

III. NUMERICAL RESULTS

As one may notice, all the unknowns to be solved appear in the coherent and the scattering terms nonlinearly. Therefore the kinetic Bloch equations have to be solved self-consistently to obtain the electron distribution and the spin coherence.

We numerically solve the kinetic Bloch equations in such self-consistent fashion to obtain temporal evolution of the electron distribution functions $f_{\mathbf{k}\sigma}(t)$ and the spin coherence

TABLE I. Material parameters used in the numerical calculations.

κ_∞	10.8	κ_0	12.9
ω_0	35.4 meV	m^*	$0.067m_0$
Δ	0.341 eV	E_g	1.55 eV
g	0.44		

$\rho_{\mathbf{k}}(t)$. Once these quantities are obtained, we are able to deduce all the quantities such as electron mobility μ and hot-electron temperature T_e for small spin polarization P as well as the spin dephasing rate for any spin polarization P. The mobility is given by $\mu=\Sigma_{\mathbf{k}\sigma}f_{\mathbf{k}\sigma}(0)\mathbf{k}/(m^*N_eE)$; the electron temperature is obtained by fitting the Boltzmann tail of the electron distribution function, whereas the spin dephasing rate is determined by the slope of the envelope of the incoherently summed spin coherence $\rho(t)=\Sigma_{\mathbf{k}}|\rho_{\mathbf{k}}(t)|$.[13,30,39] It should be noted that the spin dephasing time obtained in this way includes both the single-particle and the many-body spin dephasing contributions.

We include the electron–electron, the electron–phonon and the electron–impurity scattering throughout our computation. For electron–phonon scattering, since we concentrate on the relatively high temperature regime, only electron–longitudinal optical (LO) phonon scattering is important. The numerical scheme for solution of the kinetic equations is laid out in detail in Appendix B. The total electron density N_e, the width of the QW a and the magnetic field applied are taken to be 4×10^{11} cm^{-2}, 15 nm and 4 T, respectively. The material parameters of GaAs are listed in Table I. The numerical results are presented in Figs. 1–5.

A. Electric field dependence of the spin precession frequency

In Fig. 1 we plot the typical temporal evolution of the electron densities of spin up and down for a GaAs QW with initial spin polarization $P=2.5\%$ under two electric fields, $E=0.5$ and -0.5 kV/cm, at $T=120$ K. $B=4$ T for both cases. The corresponding incoherently summed spin coherence is also plotted in Fig. 1. One can see that the temporal evolutions of the electron densities and the spin coherence are similar to those in the absence of an applied electric field.[17]

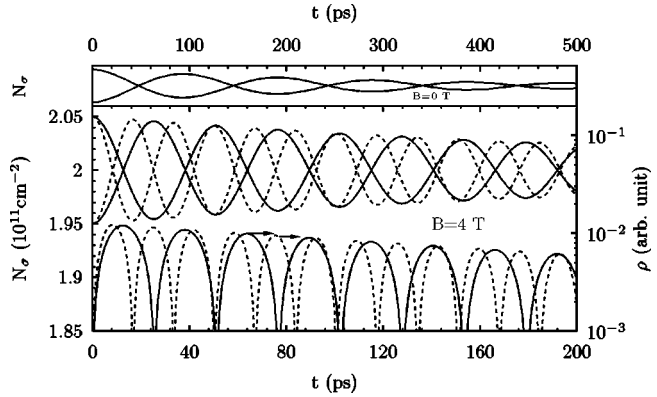

FIG. 1. Electron densities of spin up and down and the incoherently summed spin coherence ρ vs time t for a GaAs QW with initial spin polarization $P=2.5\%$ under different electric fields, $E=0.5$ (solid lines) and -0.5 kV/cm (dashed lines). Top panel: $B=0$ T; bottom panel: $B=4$ T. Note the scale of the spin coherence is on the right side and the scale of the top panel is different from that of the bottom one.

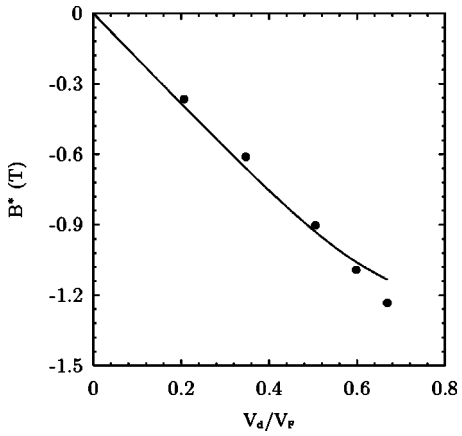

FIG. 2. Net effective magnetic field B^* from the DP term vs drift velocity V_d at $T=120$ K with impurity density $N_i=0$. The solid curve is the corresponding result from Eq. (7).

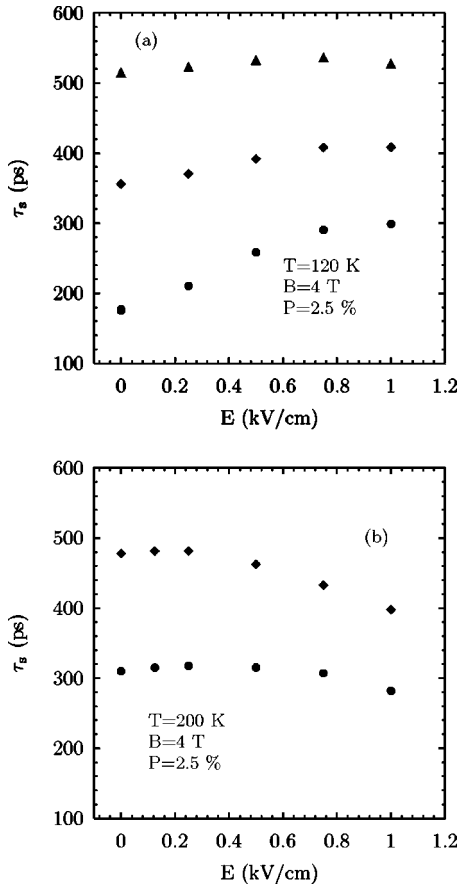

FIG. 3. SDT τ_s vs the electric field E applied at $T=$ (a) 120 and (b) 200 K for initial spin polarization $P=2.5\%$ with different impurity densities: ● $N_i=0$; ♦ $N_i=0.6\,N_e$; and ▲ $N_i=1.2\,N_e$.

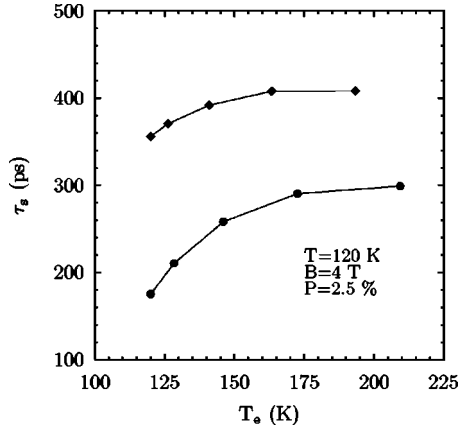

FIG. 4. SDT τ_s vs electron temperature T_e at lattice temperature $T=120$ K with initial spin polarization $P=2.5\%$ for $N_i=0$ (●) and $N_i=0.6\ N_e$ (◆). The curves are plotted as a guide to the eye.

The electron densities and the spin coherence oscillate as electron spins and undergo Larmor precession around the total (effective) magnetic field. Due to spin dephasing, the amplitude of the oscillation decays exponentially. An interesting effect of the high in-plane electric field on spin precession is that there is a marked difference in the precession frequency under different electric fields (even electric fields of the same magnitude but in opposite directions). As shown in Fig. 1, although there is almost no difference in corresponding spin dephasing rate, the periods of the oscillations are 51.2 and 33.6 ps for applied electric fields of $E=-0.5$ and 0.5 kV/cm, respectively. Both periods deviate from 40.6 ps, which is the electric-field-free one of Larmor precession under magnetic field $B=4$ T.

Moreover, it is expected that at *very low* temperature (i.e., a few kelvin) where the momentum collision rate is small, the DP term can result in rapidly damped oscillations in the spin signal when $B=0$. At higher temperatures, due to the higher collision rates these oscillations disappear totally and the spin polarization decays exponentially over time[40] and the oscillations can only be seen when there is a magnetic field applied in the Vogit configuration. Nevertheless, it is of particular interest to note in the top panel of Fig. 1 that even at temperature as high as 120 K, the spin signal oscillates with period 219.9 ps when there is *no* magnetic field applied but an applied electric field $E=0.5$ kV/cm.

Both features above originate from the high electric field **E** applied along the x axis. With the applied electric field, the electrons get a net center-of-mass drift velocity V_d and the distribution function is no longer first-order momentum free, i.e., $(1/N_e)\Sigma_{\mathbf{k}} \mathbf{k} f_{\mathbf{k}\sigma}=m^* V_d \neq 0$. From Eq. (2) one finds that there is a net effective magnetic field B^* along the x axis from the DP term which does not exist when $E=0$. From the period of spin oscillation in Fig. 1, one can deduce effective magnetic field B^*. When electric field $E=\pm 0.5$ kV/cm, the net effective magnetic field $B^*=\mp 0.74$ T.

The average of the total effective magnetic field the electrons experience at low spin polarization can be given approximately by

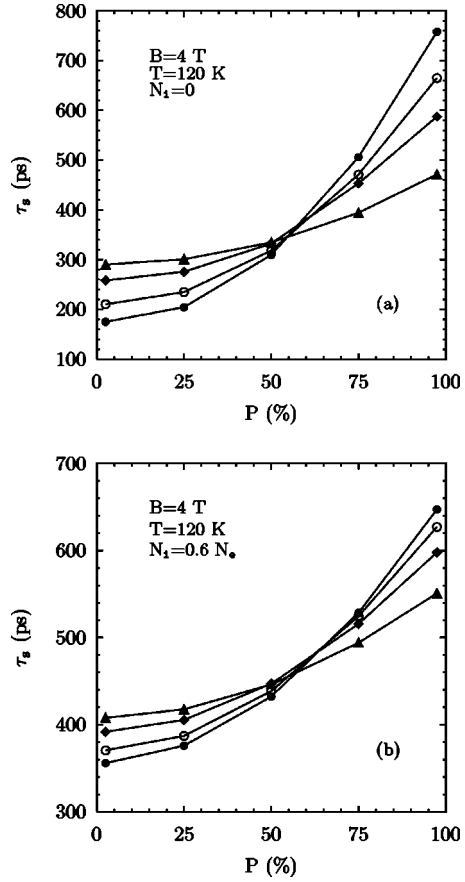

FIG. 5. Spin dephasing time τ_s (•) vs the initial spin polarization for $T=120$ K and $N_i=0$ (a) and $N_i=0.6\ N_e$ (b) under different electric fields: ● $E=0$; ○ $E=0.25$ kV/cm; ◆ $E=0.5$ kV/cm; ▲ $E=0.75$ kV/cm.

$$\mathbf{B}_{\mathrm{tot}} = \mathbf{B} + \mathbf{B}^* = \mathbf{B} + \frac{1}{g\mu_B} \frac{\int d\mathbf{k}(f_{\mathbf{k}1/2} - f_{\mathbf{k}-1/2})\mathbf{h}(\mathbf{k})}{\int d\mathbf{k}(f_{\mathbf{k}1/2} - f_{\mathbf{k}-1/2})}. \quad (6)$$

By taking the electron distribution function as the drifting Fermi function $f_{\mathbf{k}\sigma}=\{\exp[(\mathbf{k}-m^*\mathbf{V}_d)^2/(2m^*-\mu_\sigma)/(k_B T_e)] +1\}^{-1}$, the effective magnetic field for small spin polarization can be roughly estimated as follows:

$$B^* = \gamma m^{*3} V_d \{E_f/[2(1-e^{-E_f/k_B T_e})] - E_c\}/g\mu_B, \quad (7)$$

with E_f and E_c the Fermi energy and confinement energy of the QW, respectively. In Fig. 2 the effective magnetic field B^* deduced from the frequencies of our numerical result is plotted as a function of drift velocity V_d for the impurity-free sample. The result predicted by Eq. (7) is also plotted Fig. 2 for comparison with the hot-electron temperature T_e obtained by fitting the Boltzmann tail of the calculated electron distribution functions. It is seen in Fig. 2 that Eq. (7) gives a reasonable estimate of B^*.

B. Electric field dependence of the spin dephasing time of electrons with small spin polarization

In addition to affecting the spin precession frequency, the high electric field applied also changes the spin dephasing time (SDT), i.e., the inverse of the spin dephasing rate, although the electric field does not couple to the electron spin directly. In Figs. 3(a) and 3(b), we plot the SDT of the electrons with initial spin polarization $P=2.5\%$ as a function of electric field E for different impurity densities N_i at $T=120$ and 200 K, respectively. It is seen from Fig. 3(a) that for the impurity-free sample, the SDT first increases with the electric field from $\tau_s=175$ ps at $E=0$ and then saturates to $\tau_s=300$ ps, 70% higher when E is close to 1 kV/cm. For samples with impurities, the SDT also increases with the electric field but at a decreased rate of increase for higher impurity densities. When the impurity density rises to $1.2N_e$, τ_s first increases for a small electric field and then decreases when the electric field is higher than 0.75 kV/cm. Moreover the change of SDT with the electric field is much smaller than that of the impurity-free sample. The electric field dependence of the SDT varies as the background temperature changes. When the temperature is raised to a relatively high one, say, $T=200$ K in Fig. 3(b), the SDT increases slightly with the electric field and then decreases when $E>0.25$ kV/cm even for the impurity-free sample.

The electric field dependence of the SDT is understood due to the concurrent effects of the high electric field and the DP term. The most obvious effect of the electric field is that the electrons get center-of-mass drift velocity and the center of the distribution functions drift away from $\mathbf{k}=0$. One consequence of drift is that the DP term gives a net effective magnetic field as discussed above. This field is moderate and hence has little effect on the SDT. Another effect is that because more electrons are distributed in the large momentum region, the contribution from the DP term with large momentum is enhanced and the SDT can be reduced. Nevertheless, in addition to drift, the high electric field also has another countereffect: As the high electric field gives the hot-electron effect with electron temperature T_e higher than T, the scattering is strengthened. This can enhance the SDT.[8,17] In short, drift of the center of mass in momentum space tends to reduce the SDT while the hot-electron effect helps to enhance it in the regime of our study. With these two effects considered, the electric field dependence of the SDT can be understood.

When the electric field is small, its effect on the DP term due to drift is marginal. Therefore the SDT increases with the electric field due to the hot-electron effect when temperature T is relatively low. As the electric field increases, the effect of drift becomes important and the SDT saturates as a consequence. It should be noted that the hot-electron effect is more pronounced for the system with smaller impurity density under a given electric field.[41] As a result, the SDT increases more slowly with the electric field when the impurity density is higher. For high impurity-doped samples, the hot-electron effect is markedly smaller than that for pure ones, therefore the SDT only increases slightly in the low electric field region and then decreases as the effect of drift becomes more dominant. Moreover, when lattice temperature T increases, the hot-electron effect is also reduced. Therefore, in the high temperature regime the drift effect becomes important even for low electric fields and it is then possible that the SDT may drop with an increase of electric field even for impurity-free QWs. Moreover, the change in the τ_s-E curve at high temperatures is smaller than that at low temperatures as shown in Fig. 3.

We note that the electric-field dependence of τ_s we obtain is different from that of quantum wires where the SDT decreases with the electric field.[27] This difference may come from different contributions of drift and the hot-electron effect in quantum wells and quantum wires. In quantum wires the electrons are much more easily accelerated by the electric field toward higher momentum states. Therefore the drift effect is more pronounced and it is possible that the SDT is reduced by the electric field. The competing effect of drift and hot electrons in QWs results in a more complicated dependence of the SDT on the electric field.

In order to further elucidate the effect of the high electric field to the SDT, we replot the the SDT as a function of electron temperature T_e with $T=120$ K for $N_i=0$ and $0.1\ N_e$ in Fig. 4. It is seen that the SDT increases with electron temperature T_e, similar to in the electric-field-free case where the SDT increases with the temperature.[17,42] Figure 4 also shows that the impurities reduce the hot-electron effect and increase the SDT. These results indicate that for the electric fields in our study, the electric field dependence of the SDT is affected mainly by the hot-electron effect not the drift effect.

C. Electric field dependence of the spin dephasing time of electrons with high spin polarization

We now turn to studying the effect of the electric field on spin dephasing with high initial spin polarization. A similar problem *in the absence* of electric field has been studied in our previous work.[17]

The numerical results are presented in Fig. 5 where the SDT is plotted as a function of the initial spin polarization under different electric fields. It is seen that for all the electric fields we study, the SDT increases with the spin polarization as in the case of $E=0$.[17] However the speed of the increment drops with an increase of electric field. It is interesting to see that the electric field dependence of the SDT is quite different for different initial spin polarizations. In the low polarization regime, the SDT increases with the electric field while in the high polarization one, it decreases with the electric field. For moderate spin polarized electrons, the SDT is insensitive to the electric field.

The rise of the SDT with the initial spin polarization is understood by the effective magnetic field from the Hartree–Fock (HF) term. Since one component of this effective field is along the z axis, it removes "detuning" of the spin flip between the spin-up and -down bands and consequently suppresses spin precession around the magnetic field and greatly reduces spin dephasing.[17] Therefore, all the factors, such as the magnetic field, temperature, impurity, electron density, and applied electric field which can change the HF term,

affect spin dephasing in the high spin polarization case dramatically. These factors except that of the electric field have been discussed in detail in our previous work.[17] As for the applied high electric field, both the drift and the hot-electron effects affect the HF term. Drift of the center of mass in momentum space provides two competing effects on the HF term: One is to enhance the HF term through the net effective magnetic field B^* discussed above. The other is to destroy the HF term by increasing the DP effect. Meanwhile the hot-electron effect tends to soften the HF term through increases of electron temperature and the scattering rate. Our results indicate that the electric field tends to reduce the effective magnetic field from the HF term in the high spin polarization regime and as a consequence reduces the SDT.

IV. CONCLUSION

We have performed a systematic investigation of spin dephasing due to the DP mechanism in the presence of high electric fields by constructing a set of kinetic Bloch equations for *n*-type semiconductor QWs based on the nonequilibrium Green function method with gradient expansion. In our theory, we included the in-plane electric field, the magnetic field in the Voigt configuration, DP spin–orbital coupling and all spin conserving scattering such as electron–phonon, electron–nonmagnetic impurity as well as the electron–electron scattering. By numerically solving the kinetic equations, we studied the evolution of electron distribution functions and the spin coherence of spin polarized electrons. The SDT was calculated from the slope of the incoherently summed spin coherence. In this way, we were able to study in detail how spin precession and spin dephasing are affected by the electric field in various conditions, such as the impurity, temperature, and spin polarization.

The in-plane electric field has two competing effects for electron spin. The most obvious one is that the electrons get a center-of-mass drift velocity and the center of the distribution functions drifts away from $\mathbf{k}=0$. One consequence of drift is that the DP term contributes a nonvanishing net effective magnetic field which changes the period of spin precession. The larger the electric field, the larger the drift velocity and consequently the net effective magnetic field. For the electric fields we studied, the net effective magnetic field is up to the order of 1 T. This moderate magnetic field has a marginal effect on the SDT although it results in a distinct change in the spin precession period. Another consequence of drift is that because more electrons are distributed in the large momentum regime, the contribution of the DP term with large momentum is enhanced. Therefore drift can reduce the SDT. In addition to drift, the high electric field also introduces another countereffect on spin dephasing: The scattering, which tends to drive the electrons to the steady state, is enhanced because the hot-electron effect brought about by the high electric field with electron temperature T_e is higher than background T. That is, the high electric field can also affect spin dephasing through the hot-electron effect. With these two effects of the electric field on spin dephasing, the electric field dependence of spin dephasing is very rich in detail.

In the small spin polarized regime, the hot-electron effect tends to enhance the SDT since an increase in scattering rate reduces inhomogeneous broadening. Therefore in the small electric field regime where the effect of drift is marginal, the SDT increases with the electric field due to the hot-electron effect. For a larger electric field, the effect of drift become stronger. Therefore the SDT saturates under joint action of drift and the hot-electron effect. When the impurity density or background temperature T increases, the hot-electron effect is reduced and the effect of drift becomes relatively important. As a result, the increase of the SDT with the electric field is reduced. For some regimes, the SDT decreases with an increase of electric field when the drift effect is dominant.

In the high spin polarized regime where the HF term plays an important role in spin dephasing, the hot-electron effect tends to reduce the SDT since both the increase of electron temperature T_e and increase of scattering reduce the HF term. Therefore, in the high spin polarization regime, the SDT decreases with an increase of electric field.

ACKNOWLEDGMENTS

This work was supported by the Natural Science Foundation of China under Grant No. 90303012. One of the authors (M.W.W.) was supported by the "100 Person Project" of the Chinese Academy of Sciences and the Natural Science Foundation of China under Grant No. 10247002. M.Q.W. was partially supported by the China Postdoctoral Science Foundation. We would like to thank J. L. Cheng for his critical reading of this manuscript.

APPENDIX A: EFFECT OF COULOMB SCATTERING ON SPIN DEPHASING

It should be stressed that electron–electron Coulomb scattering is of particular significance in this investigation. It is not only because the Coulomb scattering is crucial in buildup of the hot-electron temperature and the hot-electron distribution functions, but also because it strongly contributes to spin dephasing with or without an electric field. With Coulomb scattering, the electron distribution functions become smoother in momentum space and electrons are distributed more uniformly around the drift center as shown in Fig. 6.

We note that treatment of electron–electron scattering in the present paper takes account of the *full effect* of Coulomb scattering which is different from in our previous work[17] where Coulomb scattering was evaluated by replacing the distribution functions and the spin coherence in scattering with corresponding isotropic averages along the angle. In this way we are able to compute the electron distribution function more accurately under high electric field and to have the hot-electron effect included in our calculation. In the absence of an applied electric field, the approximation we used before greatly reduces the CPU time and gives good qualitative results. However, this approximation is not good if one tries to get the results quantitatively.

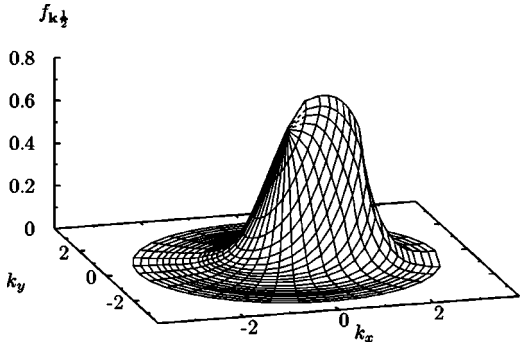

FIG. 6. Typical distribution function of spin-up electrons in the steady state with electric field $E=-0.75$ kV/cm and $P=2.5\%$.

We further show the importance of Coulomb scattering in spin dephasing by plotting the SDT as a function of the electric field applied with and without Coulomb scattering in Fig. 7. As shown in Fig. 7, for electrons with small spin polarization, Coulomb scattering tends to drive the electrons toward the equilibrium state when $E=0$ or the steady state when applied with a finite electric field, and hence greatly reduces the inhomogeneous broadening that originated from the DP term. As a result Coulomb scattering increases the SDT with /without application of an electric field. For the high spin

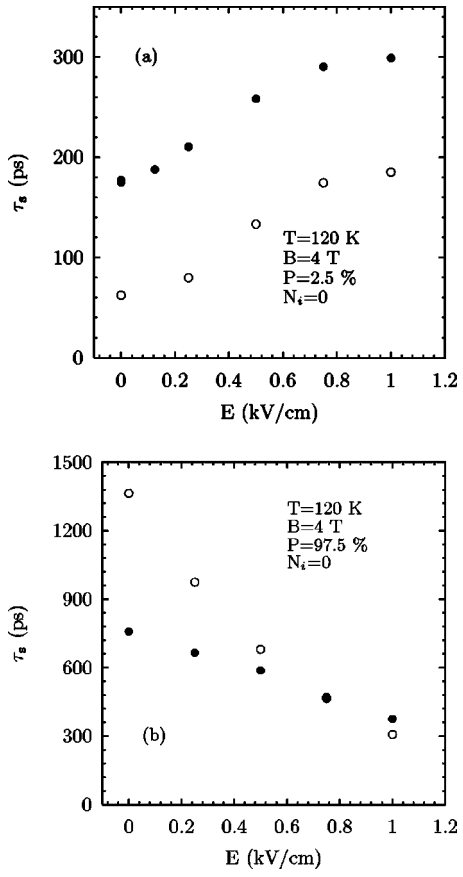

FIG. 7. Spin dephasing time in GaAs QWs with (closed circles) and without (open circles) Coulomb scattering under different spin polarizations: $P=$ (a) 2.5% and (b) 97.5%.

polarized system, as discussed earlier, the effective magnetic field along the z axis from the HF term plays a crucial role in spin dephasing and Coulomb scattering tends to reduce this effective magnetic field. Therefore the SDT becomes smaller when Coulomb scattering is included.

APPENDIX B: NUMERICAL SCHEME FOR KINETIC BLOCH EQUATIONS

Here we describe the scheme for numerical solution of the Bloch equations, Eq. (3). We first rewrite the Bloch equations as follows:

$$\dot{f}_{\mathbf{k},\sigma} = e\mathbf{E}\cdot\nabla_{\mathbf{k}} f_{\mathbf{k},\sigma} + \dot{f}_{\mathbf{k},\sigma\mathrm{coh}} + \dot{f}_{\mathbf{k},\sigma\mathrm{scat}}, \tag{B1}$$

$$\dot{\rho}_{\mathbf{k}} = e\mathbf{E}\cdot\nabla_{\mathbf{k}}\rho_{\mathbf{k}} + \dot{\rho}_{\mathbf{k}}|_{\mathrm{coh}} + \dot{\rho}_{\mathbf{k}}|_{\mathrm{scat}}. \tag{B2}$$

The coherent terms are

$$\left.\frac{\partial f_{\mathbf{k},\sigma}}{\partial t}\right|_{\mathrm{coh}} = -2\sigma\{[g\mu_B B + h_x(\mathbf{k})]\mathrm{Im}\rho_{\mathbf{k}} + h_y(\mathbf{k})\mathrm{Re}\rho_{\mathbf{k}}\} + 4\sigma\mathrm{Im}\sum_{\mathbf{q}} V_{\mathbf{q}}\rho^*_{\mathbf{k}+\mathbf{q}}\rho_{\mathbf{k}}, \tag{B3}$$

$$\left.\frac{\partial \rho_{\mathbf{k}}}{\partial t}\right|_{\mathrm{coh}} = \frac{1}{2}[ig\mu_B B + ih_x(\mathbf{k}) + h_y(\mathbf{k})](f_{\mathbf{k}1/2} - f_{\mathbf{k}-1/2}) + i\sum_{\mathbf{q}} V_{\mathbf{q}}[(f_{\mathbf{k}+\mathbf{q}1/2} - f_{\mathbf{k}+\mathbf{q}-1/2})\rho_{\mathbf{k}} - \rho_{\mathbf{k}+\mathbf{q}}(f_{\mathbf{k}1/2} - f_{\mathbf{k}-1/2})]. \tag{B4}$$

In these equations $V_{\mathbf{q}}=\Sigma_{q_z}\{4\pi e^2/\kappa_0[\mathbf{q}^2+q_z^2+\kappa^2]\}|I(iq_z)|^2$ with κ_0 the static dielectric constant and $\kappa^2=6\pi N_e e^2/(aE_f)$ the screening constant. The form factor $|I(iq_z)|^2 = \pi^4\sin^2 y/[y^2(y^2-\pi^2)^2]$ with $y=q_z a/2$. The scattering terms are

$$\begin{aligned}\left.\frac{\partial f_{\mathbf{k},\partial}}{\partial t}\right|_{\mathrm{scat}} = \Bigg\{ & -2\pi\sum_{\mathbf{q}q_z\lambda} g^2_{\mathbf{q}\lambda}\delta(\varepsilon_{\mathbf{k}} - \varepsilon_{\mathbf{k}-\mathbf{q}} - \Omega_{\mathbf{q}q_z\lambda})[N_{\mathbf{q}q_z\lambda}(f_{\mathbf{k}\sigma} \\ & - f_{\mathbf{k}-\mathbf{q}\sigma}) + f_{\mathbf{k}\sigma}(1-f_{\mathbf{k}-\mathbf{q}\sigma}) - \mathrm{Re}(\rho_{\mathbf{k}}\rho^*_{\mathbf{k}-\mathbf{q}})] \\ & - 2\pi N_i\sum_{\mathbf{q}} U^2_{\mathbf{q}}\delta(\varepsilon_{\mathbf{k}} - \varepsilon_{\mathbf{k}-\mathbf{q}})[f_{\mathbf{k}\sigma}(1-f_{\mathbf{k}-\mathbf{q}\sigma}) \\ & - \mathrm{Re}(\rho_{\mathbf{k}}\rho^*_{\mathbf{k}-\mathbf{q}})] - 2\pi\sum_{\mathbf{q}k'\sigma'} V^2_{\mathbf{q}}\delta(\varepsilon_{\mathbf{k}-\mathbf{q}} - \varepsilon_{\mathbf{k}} + \varepsilon_{\mathbf{k}'} \\ & - \varepsilon_{\mathbf{k}'-\mathbf{q}})\Big[(1-f_{\mathbf{k}-\mathbf{q}\sigma})f_{\mathbf{k}\sigma}(1-f_{\mathbf{k}'\sigma'})f_{\mathbf{k}'-\mathbf{q}\sigma'} \\ & + \frac{1}{2}\rho_{\mathbf{k}}\rho^*_{\mathbf{k}-\mathbf{q}}(f_{\mathbf{k}'\sigma'} - f_{\mathbf{k}'-\mathbf{q}\sigma'}) + \frac{1}{2}\rho_{\mathbf{k}'}\rho^*_{\mathbf{k}'-\mathbf{q}} \\ & \times(f_{\mathbf{k}-\mathbf{q}\sigma} - f_{\mathbf{k}\sigma})\Big]\Bigg\} - \{\mathbf{k}\leftrightarrow\mathbf{k}-\mathbf{q}, \mathbf{k}'\leftrightarrow\mathbf{k}'-\mathbf{q}\},\end{aligned} \tag{B5}$$

$$\left.\frac{\partial \rho_{\mathbf{k}}}{\partial t}\right|_{\text{scat}} = \Bigg\{ \pi \sum_{\mathbf{q}q_z\lambda} g^2_{\mathbf{q}q_z\lambda}\delta(\varepsilon_{\mathbf{k}}-\varepsilon_{\mathbf{k}-\mathbf{q}}-\Omega_{\mathbf{q}q_z\lambda})[\rho_{\mathbf{k}-\mathbf{q}}(f_{\mathbf{k}1/2}+f_{\mathbf{k}-1/2})+(f_{\mathbf{k}-\mathbf{q}1/2}+f_{\mathbf{k}-\mathbf{q}-1/2}-2)\rho_{\mathbf{k}}-2N_{\mathbf{q}q_z\lambda}(\rho_{\mathbf{k}}-\rho_{\mathbf{k}-\mathbf{q}})]$$

$$+\pi N_i \sum_{\mathbf{q}} U^2_{\mathbf{q}}\delta(\varepsilon_{\mathbf{k}}-\varepsilon_{\mathbf{k}-\mathbf{q}})[(f_{\mathbf{k}1/2}+f_{\mathbf{k}-1/2})\rho_{\mathbf{k}-\mathbf{q}}-(2-f_{\mathbf{k}-\mathbf{q}1/2}-f_{\mathbf{k}-\mathbf{q}-1/2})\rho_{\mathbf{k}}]-\sum_{\mathbf{q}k'}\pi V^2_{\mathbf{q}}\delta(\varepsilon_{\mathbf{k}-\mathbf{q}}-\varepsilon_{\mathbf{k}}+\varepsilon_{\mathbf{k}'}-\varepsilon_{\mathbf{k}'-\mathbf{q}})$$

$$\times((f_{\mathbf{k}-\mathbf{q}1/2}\rho_{\mathbf{k}}+\rho_{\mathbf{k}-\mathbf{q}}f_{\mathbf{k}-1/2})(f_{\mathbf{k}'1/2}-f_{\mathbf{k}'-\mathbf{q}1/2}+f_{\mathbf{k}'-1/2}-f_{\mathbf{k}'-\mathbf{q}-1/2})+\rho_{\mathbf{k}}[(1-f_{\mathbf{k}'1/2})f_{\mathbf{k}'-\mathbf{q}1/2}+(1-f_{\mathbf{k}'-1/2})f_{\mathbf{k}'-\mathbf{q}-1/2}$$

$$-2\mathrm{Re}(\rho^*_{\mathbf{k}'}\rho_{\mathbf{k}'-\mathbf{q}})]-\rho_{\mathbf{k}-\mathbf{q}}[f_{\mathbf{k}'1/2}(1-f_{\mathbf{k}'-\mathbf{q}1/2})+f_{\mathbf{k}'-1/2}(1-f_{\mathbf{k}'-\mathbf{q}-1/2})-2\mathrm{Re}(\rho^*_{\mathbf{k}'}\rho_{\mathbf{k}'-\mathbf{q}})]\Bigg)-\{\mathbf{k}\leftrightarrow\mathbf{k}-\mathbf{q},\mathbf{k}'\leftrightarrow\mathbf{k}'-\mathbf{q}\}, \tag{B6}$$

in which $\{\mathbf{k}\leftrightarrow\mathbf{k}-\mathbf{q},\mathbf{k}'\leftrightarrow\mathbf{k}'-\mathbf{q}\}$ stands for the same terms previously in { } but interchanging $\mathbf{k}\leftrightarrow\mathbf{k}-\mathbf{q}$ and $\mathbf{k}'\leftrightarrow\mathbf{k}'-\mathbf{q}$. In these equations $g_{\mathbf{q},q_z,\lambda}$ are the matrix elements of electron–phonon coupling for mode λ. For LO phonons, $g^2_{\mathbf{q}q_z\mathrm{LO}}=\{4\pi\alpha\Omega^{3/2}_{\mathrm{LO}}/[\sqrt{2\mu}(q^2+q_z^2)]\}|I(iq_z)|^2$ with $\alpha=e^2\sqrt{\mu/(2\Omega_{\mathrm{LO}})}(\kappa_\infty^{-1}-\kappa_0^{-1})$. κ_∞ is the optical dielectric constant and Ω_{LO} is the LO-phonon frequency. $N_{\mathbf{q}q_z\lambda}=1/[\exp(\Omega_{\mathbf{q}q_z\lambda}/k_BT)-1]$ is the Bose distribution function of the phonon with mode λ at temperature T. $U^2_{\mathbf{q}}=\Sigma_{q_z}\{4\pi Z_i e^2/[\kappa_0(q^2+q_z^2)]\}^2|I(iq_z)|^2$ is the electron–impurity interaction matrix element with Z_i the charge number of the impurity. Z_i is assumed to be 1 throughout our calculation.

For numerical calculation, one first turns the Bloch equations into discrete ones. To facilitate evaluation of the energy conservation, i.e., the δ function in the scattering terms, we divide the truncated 2D momentum space into $N\times M$ control regions, each with equal energy and angle intervals as shown in Fig. 8. The **k**-grid points are chosen to be the center of each control region and therefore are written as

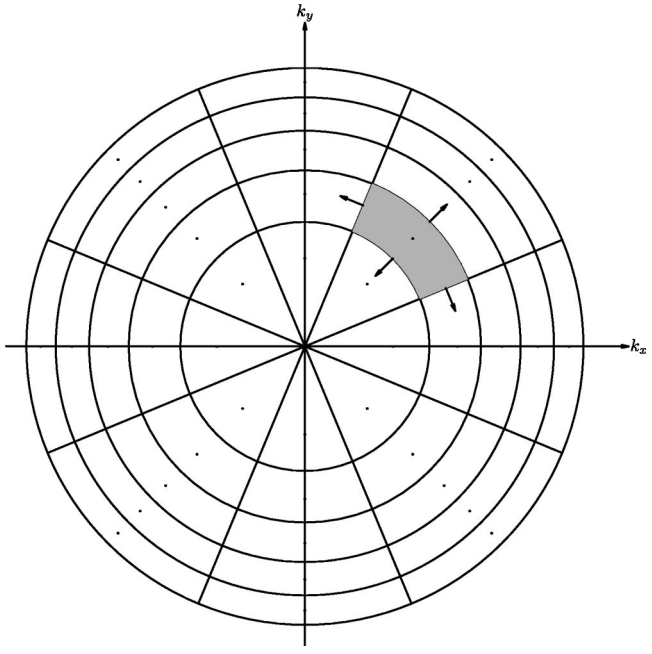

FIG. 8. Discrete momentum space.

$$\mathbf{k}_{n,m}=\sqrt{2m^*E_n}(\cos\,\theta_m,\sin\,\theta_m), \tag{B7}$$

with $E_n=(n+1/2)\Delta E$ and $\theta_m=m\Delta\theta$. Here $n=0,1,\ldots,N-1$ and $m=0,1,\ldots,M-1$ with $E_{N-1}=E_{\mathrm{cut}}$, the truncation energy, and $\theta_{M-1}=(M-1)2\pi/M$.

In order to carry out integration of the δ function in the scattering term, ΔE has to be chosen to satisfy $\Omega_0=n_{\mathrm{LO}}\Delta E$ [or $\Omega_0=(n_{\mathrm{LO}}+\frac{1}{2})\Delta E$]. In this scheme, the coherent terms and the scattering terms of electron–impurity and electron-phonon scattering can be divided into discrete ones directly. Nevertheless $f_{\mathbf{k}\sigma}$ and $\rho_{\mathbf{k}}$ in the Coulomb scattering terms are not all on the grid points we choose. We approximate them to be interpolation of the nearest grid points with the same energy.

The driving terms should be treated with caution because the equations are stable only for some finite differential schemes, such as forward differencing and center differencing schemes. In this study, we use the forward differencing scheme. However, the usual expression for this scheme is based on Taylor series expansion and is difficult to apply to the polar coordinate system which we use in this work. This difficult can be circumvented by the so-called discrete conservation principle:[43]

$$\begin{aligned} e\mathbf{E}\cdot\nabla_{\mathbf{k}}f_{\mathbf{k},\sigma}|_{\mathbf{k}=\mathbf{k}_{n,m}} &\simeq \frac{\int_{\Omega_{n,m}} d^2k e\mathbf{E}\cdot\nabla_{\mathbf{k}}f_{\mathbf{k},\sigma}}{m^*\Delta E\Delta\theta} \\ &= \frac{1}{m^*\Delta E\Delta\theta}\int_{\partial\Omega_{n,m}} ds e\mathbf{E}\cdot\hat{\mathbf{n}}f_{\mathbf{k},\sigma} \\ &= \frac{1}{m^*\Delta E\Delta\theta}\sum_{n'm'}\int_{\Omega_{n,m}\cap\Omega_{n',m'}} ds e\mathbf{E}\cdot\hat{\mathbf{n}}f_{\mathbf{k},\sigma} \\ &\simeq \frac{1}{m^*\Delta E\Delta\theta}\sum_{n'm'} e\mathbf{E}\cdot\hat{\mathbf{n}}^{n'm'}_{n,m}s^{n'm'}_{n,m}f_{\mathbf{k}'_{nm},\sigma}. \end{aligned} \tag{B8}$$

Here $\Omega_{n,m}$ and $\partial\Omega_{n,m}$ are control regions which contain grid point $\mathbf{k}_{n,m}$ and the corresponding boundary. In the last step of the above equation, integration of the boundary is replaced

by summation over the first-order quadrature on the four (or three if the control region is a neighbor of $\mathbf{k}=0$) sides of the boundary $\partial\Omega_{n,m}$ with $s_{n,m}^{n'm'}$ and $\hat{\mathbf{n}}_{n,m}^{n'm'}$, respectively, the length and the outward normal to boundary $\Omega_{nm}\cap\Omega_{n'm'}$. In order to satisfy the need for numerical stability, $\mathbf{k}'_{n,m}$ is chosen to be $\mathbf{k}_{n,m}$ if $-e\mathbf{E}\cdot\hat{\mathbf{n}}_{nm}^{n'm'}>0$ and $\mathbf{k}_{n',m'}$ otherwise.

We note that this choice of $\mathbf{k}$ makes our approach identical to the forward differencing scheme. The time evolution is computed by the fourth-order Runge–Kutta method.[44] Computation is carried out in a parallel manner in the "Beowulf" cluster. For a typical calculation, it takes about 7.5 h to get one SDT with 16-node AMD Athlon XP2800+CPUs when both N and M are chosen to be 32.

*Corresponding author. Mailing address: Department of Physics, University of Science and Technology of China, Hefei, Anhui 230026, China. Electronic address: mwwu@ustc.edu.cn

[1] S. A. Wolf, J. Supercond. **13**, 195 (2000).
[2] *Spin Electronics*, edited by M. Ziese and M. J. Thornton (Springer, Berlin, 2001).
[3] E. M. Conwell, *Solid State Physics* (Academic, New York, 1967), Vol. Suppl. 9.
[4] E. M. Conwell, *High Field Transport in Semiconductors* (Pergamon, Oxford, 1972).
[5] J. M. Kikkawa, I. P. Smorchkova, N. Samarth, and D. D. Awschalom, Science **277**, 1284 (1997); J. M. Kikkawa and D. D. Awschalom, Nature (London) **397**, 139 (1998); Phys. Rev. Lett. **80**, 4313 (1998).
[6] H. Ohno, Science **281**, 951 (1998);Y. Ohno, R. Terauchi, T. Adachi, F. Matsukura, and H. Ohno, Phys. Rev. Lett. **83**, 4196 (1999).
[7] R. I. Dzhioev, B. P. Zakharchenya, V. L. Korenev, D. Gammon, and D. S. Katzer, JETP Lett. **74**, 182 (2001); R. I. Dzhioev, K. V. Kavokin, V. L. Korenev, M. V. Lazarev, B. Y. Meltser, M. N. Stepanova, B. P. Zakharchenya, D. Gammon, and D. S. Katzer, Phys. Rev. B **66**, 245204 (2002).
[8] *Optical Orientation*, edited by F. Meier and B. P. Zakharchenya (North-Holland, Amsterdam, 1984).
[9] Y. Yafet, Phys. Rev. **85**, 478 (1952).
[10] R. J. Elliot, Phys. Rev. **96**, 266 (1954).
[11] G. L. Bir, A. G. Aronov, and G. E. Pikus, Zh. Eksp. Teor. Fiz. **69**, 1382 (1975) [Sov. Phys. JETP **42**, 705 (1975)].
[12] M. I. D'yakonov and V. I. Perel', Zh. Eksp. Teor. Fiz. **60**, 1954 (1971) [Sov. Phys. JETP **33**, 1053 (1971)].
[13] M. W. Wu and C. Z. Ning, Eur. Phys. J.: Appl. Phys. **18**, 373 (2000); M. W. Wu, J. Supercond. **14**, 245 (2001); cond-mat/0109258 (2001).
[14] M. W. Wu and C. Z. Ning, Phys. Status Solidi B **222**, 523 (2000).
[15] M. W. Wu, J. Phys. Soc. Jpn. **70**, 2195 (2001).
[16] M. W. Wu and M. Kuwata-Gonokami, Solid State Commun. **121**, 509 (2002).
[17] M. Q. Weng and M. W. Wu, Phys. Rev. B **68**, 075312 (2003); J. Phys.: Condens. Matter **15**, 5563 (2003); Phys. Status Solidi B **239**, 121 (2003); J. L. Cheng, M. Q. Weng, and M. W. Wu, Solid State Commun. **128**, 365 (2003).
[18] D. Hägele, M. Oestreich, W. W. Rühle, N. Nestle, and K. Eberl, Appl. Phys. Lett. **73**, 1580 (1998).
[19] H. Sanada, I. Arata, Y. Ohno, Z. Chen, K. Kayanuma, Y. Oka, F. Matsukura, and H. Ohno, Appl. Phys. Lett. **81**, 2788 (2002).
[20] I. Malajovich, J. J. Berry, N. Samarth, and D. D. Awschalom, Nature (London) **411**, 770 (2001).
[21] G. Schmidt, D. Ferrand, L. W. Molenkampt, A. T. Filip, and B. J. van Wees, Phys. Rev. B **62**, R4790 (2000).
[22] Y. Qi and S. Zhang, Phys. Rev. B **67**, 052407 (2003).
[23] A. Bournel, P. Dollfus, P. Bruno, and P. Hesto, Ultrafast Phenomena in Semiconductors Materials Science Forum 297, 205 (1999); Physica B **272**, 331 (1999); Solid State Commun. **104**, 85 (1997).
[24] S. Saikin, M. Shen, M.-C. Cheng, and V. Privman, J. Appl. Phys. **94**, 1769 (2003).
[25] M. Shen, S. Saikin, M.-C. Cheng, and V. Privman, Math. Comput. Simulation **65**, 351 (2004).
[26] S. Pramanik, S. Bandyopadhyay, and M. Cahay, Appl. Phys. Lett. **84**, 266 (2004).
[27] S. Pramanik, S. Bandyopadhyay, and M. Cahay, Phys. Rev. B **68**, 075313 (2003).
[28] Y. A. Bychkov and E. I. Rashba, J. Phys. C **17**, 6039 (1984); JETP Lett. **39**, 78 (1984).
[29] E. I. Rashba and A. L. Efros, Appl. Phys. Lett. **83**, 5295 (2003).
[30] M. W. Wu and H. Metiu, Phys. Rev. B **61**, 2945 (2000).
[31] M. Q. Weng and M. W. Wu, Phys. Rev. B **66**, 235109 (2002); J. Appl. Phys. **93**, 410 (2003).
[32] M. Q. Weng, M. W. Wu, and Q. W. Shi, Phys. Rev. B **69**, 125310 (2004).
[33] A. P. Dmitriev, V. Y. Kachorovskii, M. S. Shur, and M. Stroscio, Solid State Commun. **113**, 565 (2000).
[34] A. P. Dmitriev, V. Y. Kachorovskii, and M. S. Shur, J. Appl. Phys. **89**, 3793 (2001).
[35] G. Dresselhaus, Phys. Rev. **100**, 580 (1955).
[36] A. G. Aronov, G. E. Pikus, and A. N. Titkov, Zh. Eksp. Teor. Fiz. **84**, 1170 (1983) [Sov. Phys. JETP **57**, 680 (1983)].
[37] G. D. Mahan, *Many-Particle Physics* (Plenum, New York, 1981).
[38] H. Haug and A. P. Jauho, *Quantum Kinetics in Transport and Optics of Semiconductors* (Springer-Verlag, Berlin, 1996).
[39] T. Kuhn and F. Rossi, Phys. Rev. Lett. **69**, 977 (1992).
[40] M. A. Brand, A. Malinowski, O. Z. Karimov, P. A. Marsden, R. T. Harley, A. J. Shields, D. Sanvitto, D. A. Ritchie, and M. Y. Simmons, Phys. Rev. Lett. **89**, 236601 (2002).
[41] X. L. Lei and C. S. Ting, Phys. Rev. B **30**, 4809 (1984).
[42] A. Malinowski, R. S. Britton, T. Grevatt, R. T. Harley, D. A. Ritchie, and M. Y. Simmons, Phys. Rev. B **62**, 13034 (2000).
[43] *Computational Science Education Project*, edited by V. Meiser (1993); electronic book, available from http://csepl.phy.ornl.gov/csep.html.
[44] W. H. Press, S. A. Teukolsky, and W. T. Vetterling, *Numerical Recipes in Fortran 77: The Art of Scientific Computing* (Cambridge University Press, Cambridge, 1988).